Journal of Structural Geology 31 (2009) 388–402

Contents lists available at ScienceDirect

Journal of Structural Geology

journal homepage: www.elsevier.com/locate/jsg

Temporal and spatial development of a gravity-driven normal fault array: Middle–Upper Jurassic, South Viking Graben, northern North Sea

C.A-L. Jackson [a,*], E. Larsen [b,1]

[a] Department of Earth Science & Engineering, Imperial College, Prince Consort Road, London, SW7 2BP, England, UK
[b] StatoilHydro ASA, Svanholmen 90, Stavanger, Norway

ARTICLE INFO

Article history:
Received 22 July 2008
Received in revised form
5 January 2009
Accepted 9 January 2009
Available online 20 January 2009

Keywords:
Rift basin
Syn-rift
North Sea
Late Jurassic
Normal faulting
Gravity-driven deformation

ABSTRACT

Three-dimensional seismic and well data from the South Viking Graben, northern North Sea Basin, is used to investigate the temporal and spatial development of a gravity-driven normal fault array above an evaporite-rich detachment. Two moderate throw (500–900 m), Middle to Upper Jurassic normal faults (the Gudrun and Brynhild Faults) are developed within the study area. Both faults die-out laterally and tip-out upwards at different structural levels within the syn-rift succession. Both faults terminate downwards into Late Permian evaporites (Zechstein Group) and do not offset pre-evaporite basement units. This thin-skinned fault array developed in response to westwards tilting of the hangingwall of the South Viking Graben during Late Jurassic rifting, and consequent westward gliding and extensional break-up of units above the mechanically-weak evaporite horizon. Isochron mapping and well-based correlation of Middle to Upper Jurassic syn-rift units allow constraints to be placed on the temporal evolution of the fault array. Several stages of structural development are observed which document; (i) a period of relatively minor, early (i.e. pre-rift) halokinesis; (ii) variable spatial activity on individual faults within the array; and (iii) the progressive upslope migration of active faulting within the array as a whole. The progressive upslope migration of fault activity is interpreted to reflect progressive "unbuttressing" and extensional faulting of upslope, post-evaporite units. The overall structural style and kinematic evolution identified here shares many characteristics with both '*rift–raft tectonics*' documented in other rifts developed above an evaporitic sub-stratum and '*raft tectonics*' described from passive margin basins containing thick mobile salt or shale intervals. This style of fault array evolution differs from that observed in rifts lacking mobile layers at-depth and highlights the importance of these units in the structural development of rifts.

1. Introduction

Gravity-driven deformation is a common process on many passive margins and leads to the development of a range of kinematically-linked extensional and compressional structures (e.g. Duval et al., 1992; Lundin, 1992; Damuth, 1994; Spathopolous, 1996; Corredor et al., 2005). Gravity-driven deformation in these settings is intimately linked to; (i) the presence of a detachment horizon at-depth which is typically evaporite or shale-dominated; and (ii) down-to-the-basin tilting, which is related to thermal subsidence and sediment loading, and which triggers gravity-induced sliding and deformation of the supra-detachment stratigraphy (see references above). Such deformation is commonly termed 'thin-skinned', indicating that deformation is stratigraphically decoupled from deeper, basement-involved processes. Thin-skinned, gravity-driven deformation is not restricted to passive margins, however, but has also been described from rift basins in areas of continental extension (Petersen et al., 1992; Penge et al., 1993, 1999; Bishop et al., 1995; Nilsen et al., 1995; Stewart and Coward 1995; Thomas and Coward, 1996; Clark et al., 1998; Stewart et al., 1999; Davies et al., 2001). In these settings, an evaporite-dominated unit forms the detachment, and tilting of this unit and subsequent supra-detachment deformation is characterised by normal faulting and reactive diapirism (so-called *rift–raft tectonics* of Penge et al., 1993, 1999). Although the geometry and temporal evolution of these structures have been relatively well-described from passive margins (e.g. Anderson et al., 2000; Rouby et al., 2002; Dutton et al., 2004), comparatively little work has focused on the

* Corresponding author. Tel.: +442075947450; fax: +442075947444.
E-mail address: c.jackson@imperial.ac.uk (C.A-L. Jackson).
[1] Current address: Rocksource ASA, Olav Kyrresgt. 22, Postboks 994, N5808, Bergen, Norway.

0191-8141/$ – see front matter © 2009 Elsevier Ltd. All rights reserved.
doi:10.1016/j.jsg.2009.01.007

detailed evolution of geometrically and kinematically similar structures developed within rifts (see Petersen et al., 1992; Penge et al., 1993, 1999 for exceptions). For example, the kinematic linkage between individual structures within the evolving fault array and the manner in which deformation migrates through time remains unclear.

The aims of this study are to: (i) describe the geometry of normal faults within a rift-related, gravity-driven fault array; and (ii) document the temporal and spatial evolution of the fault array by analysis of the architecture of coeval syn-rift deposits. To achieve these aims, 3D seismic and well data were utilised from the hangingwall of the South Viking Graben, northern North Sea Basin (Fig. 1). This is an excellent location to conduct this study due to the availability of high quality 3D seismic data with which to document the three-dimensional structural style of the fault array and associated syn-rift stratal units. In addition, well data, which is tied to a robust biostratigraphic framework, allows the age of the mapped syn-rift stratal units to be determined and the timing of structural development to be constrained. This study demonstrates that during the Late Jurassic rift event, the hangingwall of the South Viking Graben underwent thin-skinned extension related to tilting of an evaporite-dominated unit within the basin fill. Growth of individual faults by tip propagation and retreat is observed, in addition to large-scale migration of deformation between faults within the array. The results of this study have implications for the temporal and spatial evolution of gravity-driven fault arrays above an evaporite-dominated, intra-stratal detachment, the structural evolution of rifts, and the structural development of the South Viking Graben.

2. Tectono-stratigraphic evolution of the South Viking Graben

2.1. Early Permian–Late Triassic

The South Viking Graben formed in response to several periods of crustal extension through the Mesozoic. The basin has been controlled throughout this time by the Graben Boundary Fault Zone which is located along its western margin (*sensu* Cherry, 1993) (Fig. 1). The earliest period of fault-controlled subsidence is generally considered to have occurred in the Early to Late Permian (e.g. Glennie, 1984; Gabrielsen et al., 1990; Coward, 1995). During this time, the South Viking Graben was located along the northern margin of the North Permian Salt Basin, where it formed a broadly N–S-trending, fault-bounded marine embayment (e.g. Glennie, 1990; Ziegler, 1990; Hodgson et al., 1992). Within this embayment a series of evaporite-dominated units (Zechstein Group) were deposited, with anhydrite and halite-rich, 'basinal' evaporite facies in the axis of the basin passing laterally into carbonate-rich, "marginal" evaporite facies towards the basin margins (Fig. 1b) (Pegrum and Ljones, 1984; Thomas and Coward, 1996). There is seismic evidence for halokinesis both regionally (see Pegrum and Ljones, 1984; Thomas and Coward, 1996) and within the present study area, with salt pillows, diapirs and discontinuous, NNE–SSW-trending walls being developed (Figs. 1C and 3A). These structures bound sub-circular to elongate structural lows which formed due to withdrawal and migration of salt into the adjacent salt bodies. The presence of the Zechstein Group influenced the structural style associated with both the Middle–Late Jurassic extensional and latest Jurassic–Early Cretaceous compressional events (Pegrum and Ljones, 1984; Thomas and Coward, 1996; Jackson and Larsen, 2008).

During the Triassic, continental conditions prevailed in the South Viking Graben and shale-dominated (Smith Bank Formation) and sandstone-dominated (Skagerrak Formation) clastic units were deposited (Fig. 2) (Pegrum and Ljones, 1984; Fisher and Mudge, 1990, 1998; Frostick et al., 1992). Although the magnitude of extension and fault-controlled subsidence during this time is poorly-constrained, it is speculated that the Graben Boundary Fault Zone was active (e.g. Ziegler, 1990; Coward, 1995; Thomas and Coward, 1996).

2.2. Early Jurassic–Early Cretaceous

Early Jurassic units are absent within the study area due to uplift and erosion of the South Viking Graben during the latest Early Jurassic. This was associated with the formation of the Mid-North Sea Dome, the crest of which was located *ca.* 100 km to the south (Ziegler, 1990; Underhill and Partington, 1993, 1994).

During the Middle Jurassic, the Mid-North Sea Dome subsidised and major activity on the Graben Boundary Fault Zone commenced; these events resulted in rapid subsidence of the South Viking Graben (Harris and Fowler, 1987; Ziegler, 1990; Cockings et al., 1992; Coward, 1995; Thomas and Coward, 1996). The present-day geometry of the basin is dominated by structures associated with this rather than the earlier Permo-Triassic rift event (Fig. 1b and c). The South Viking Graben forms a N–S to NNE–SSW trending, gently (5–7°) westwards-dipping half-graben, which is bound to the W by the Graben Boundary Fault Zone and to the east by the Utsira High (Fig. 1b and c). The Graben Boundary Fault Zone strikes N–S to NNE–SSW, has a planar to slightly listric geometry in cross-section and has >4 km of throw (Harris and Fowler, 1987; Thomas and Coward, 1996; show [accolade2]?>5; Fletcher, 2003a,b). Previous studies suggest that activity on the Graben Boundary Fault Zone initiated in the Early or Late Callovian, with the main phase of extension and basin subsidence occurring during the Oxfordian to Middle Volgian (Cockings et al., 1992; Cherry, 1993; McClure and Brown, 1992; Fletcher, 2003a,b). Tilting of the hangingwall was responsible for thin-skinned deformation and extensional faulting of units above the Zechstein Group (Thomas and Coward, 1996) (see hangingwall faults in Figs. 1c and 3b); the structural style and evolution of these structures form the focus of this study.

During the middle and Late Jurassic, fault-controlled subsidence coupled with a eustatic rise in sea-level resulted in deposition of an upward-deepening succession within the South Viking Graben Delta-plain (Sleipner Formation) and shallow marine (Hugin Formation) deposits pass upwards into shelf deposits (Heather Formation), which are in turn overlain by deep marine deposits (Draupne Formation) (Fig. 2). Activity on the Graben Boundary Fault Zone and subsidence in the South Viking Graben waned during the Late Volgian to Ryazanian. This corresponded to the initiation of a period of compression and inversion within the South Viking Graben (e.g. Thomas and Coward, 1996; Brehm, 2003; Fletcher, 2003a,b; Jackson and Larsen, 2008). Importantly, the magnitude of inversion-related shortening was not sufficient to significantly modify the original extensional geometry of the earlier-formed faults (see Jackson and Larsen, 2008).

3. Dataset

The 3D time-migrated seismic dataset used for this study covers 370 km^2. It has an inline (N–S) and crossline (E–W) spacing of 12.5 m and a record length of 5.5 s (two-way time). The vertical axis is in milliseconds two-way time (ms TWT). Frequency analysis indicates that the vertical resolution within the interval of interest is *ca.* 30 m. Fault throw is measured in ms TWT and has been converted to metres based on interval velocity data from nearby wells; a range rather than an absolute value is presented for all measurement to account for a ±10% uncertainty in the velocities values used for depth conversion. Seismic data are displayed with a downward increase in acoustic impendence represented by

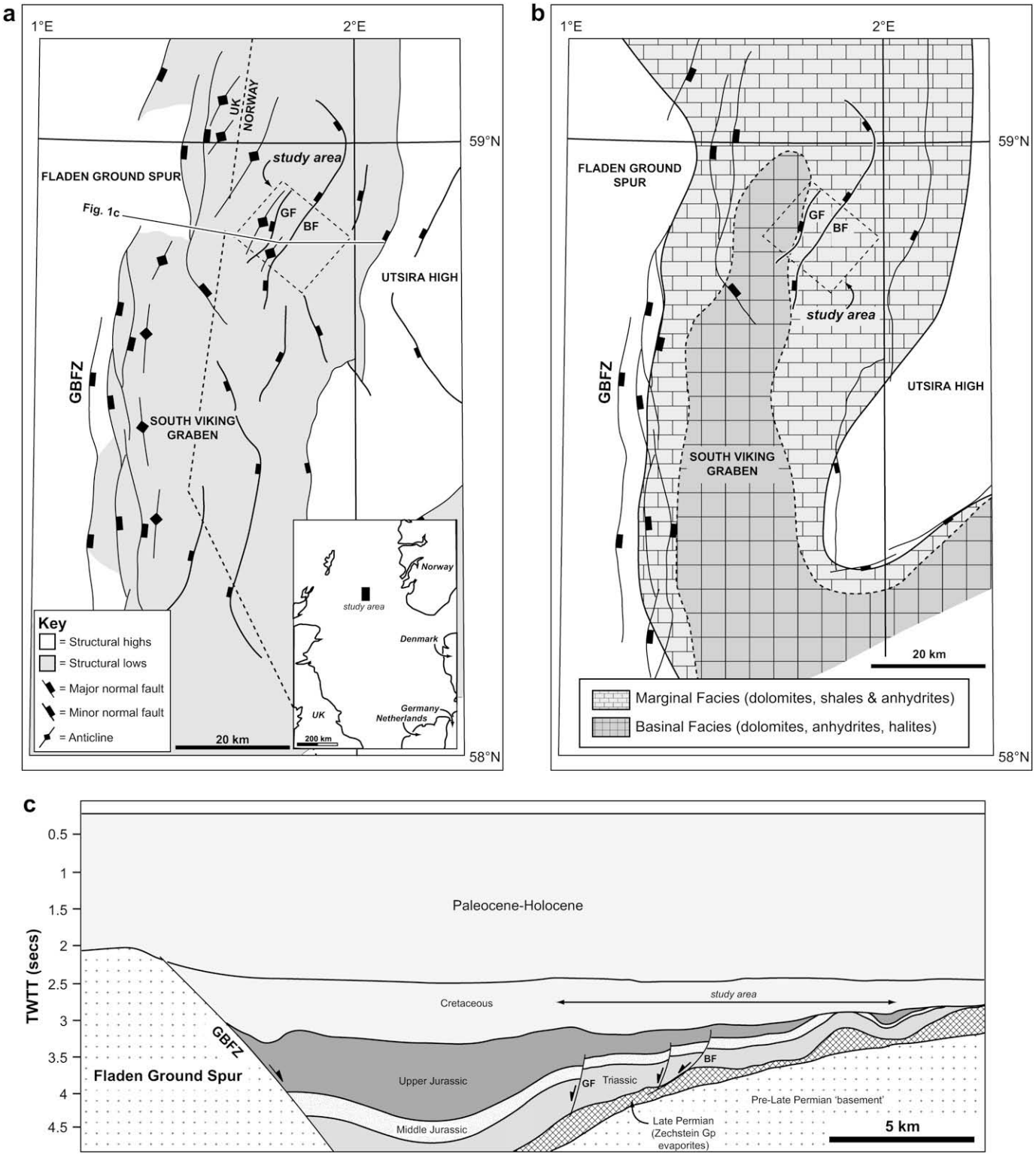

Fig. 1. (a) Simplified map illustrating the structural setting of the study area (dashed box) on the hangingwall of the South Viking Graben, offshore Norway, northern North Sea. The location of the cross-section shown in (c) is indicated. (b) Simplified map illustrating the interpreted distribution of facies within the Zechstein Group (Upper Permian). This map also serves as an approximate 'Late Permian' paleogeographic map by illustrating the occurrence of a N–S-trending marine embayment along the axis of the South Viking Graben. (c) Simplified structural cross-section across the South Viking Graben, the location of which is shown in (a). Note the development of Zechstein Group pillows and diapirs, normal faults within the Middle to Upper Jurassic supra-salt cover which detach downwards into the Zechstein Group, and inversion-related anticlines at the top of the Upper Jurassic succession. BF = Brynhild Fault; GF = Gudrun Fault; GBFZ = Graben Boundary Fault Zone.

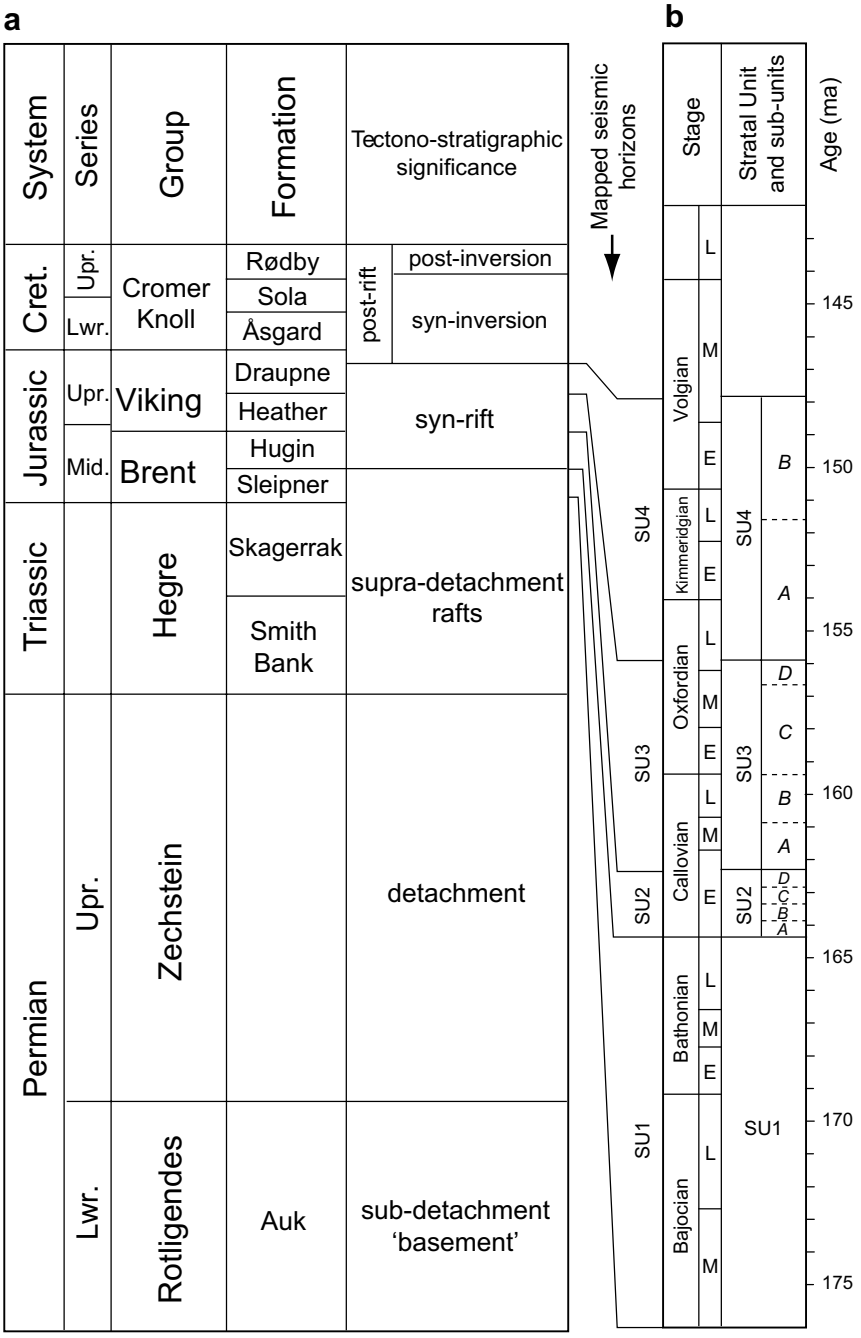

Fig. 2. (a) Composite stratigraphic column for the Norwegian sector of the northern part of the South Viking Graben. The regional tectono-stratigraphic significance of various stratigraphic units is also indicated. (b) Detailed stratigraphic column focused on the Middle to Late Jurassic, late pre-rift to syn-rift interval of interest. The stratal units (SU) and stratal sub-units (A, B, C, etc) discussed in the text are indicated. Key surfaces bounding lithostratigraphic units are shown as solid bold lines; key surfaces within lithostratigraphic units and which define sub-units are shown as thin, dashed lines. Mapped seismic reflection events and the stratal units (SU) they bound are shown as thick bold lines linking (a) and (b).

a trough (black) and a downward decrease in acoustic impedance represented by a peak (red).

Five wells containing electrical log data and with complimentary biostratigraphic reports, composite logs and original well reports, were available for this study. Three of the five wells are located immediately adjacent to one of the structures studied here (the Gudrun Fault), whereas the other two wells are located towards the basin margin (Fig. 3). Stratal thicknesses quoted in the text are true stratigraphic thicknesses, as all wells are vertical (or near-vertical) and seismic data indicate that strata are approximately horizontal or gentle-dipping ($<5^{\circ}$) at the well locations. Six age-constrained stratigraphic surfaces are identified within the interval of interest. These define major changes in lithology and are characterised by marked and abrupt changes in seismic velocity and density. Accordingly, these surfaces manifest on seismic data as relatively high-continuity, moderate to high-amplitude seismic reflection events that can be mapped over most of the study area. These reflection events bound four syn-rift stratal units which correspond to locally-defined, age-constrained, lithostratigraphic units; SU1 = Early Bajocian–Early Callovian

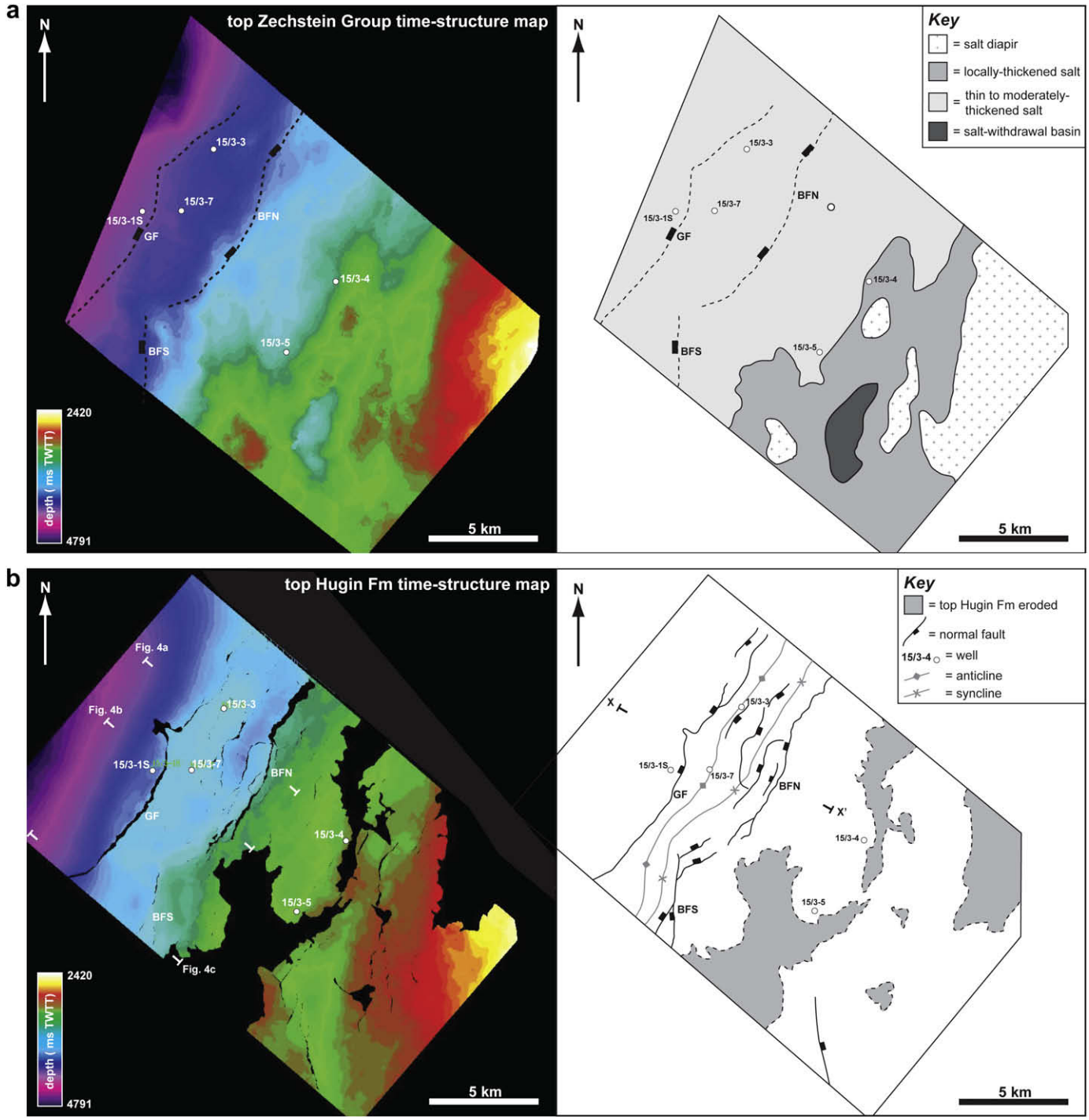

Fig. 3. (A) Time-structure map of the top of the Zechstein Group and interpretative drawing illustrating the key structures identified. In the SE of the study area note the development of diapirs, elongate salt walls and intra-salt high mini-basins. The approximate locations of Late Jurassic faults which detach above this structural level (i.e. supra-Zechstein Group faults) are shown as dashed lines. (B) Time-structure map of the top of SU2 (top Hugin Fm) and interpretative drawing illustrating the main gravity-driven, rift-related faults studied in this paper and associated folds. The locations of the seismic sections shown in Fig. 4 are shown on the time-structure map and the location of the sequential cross-sections (X–X') shown in Fig. 7 is shown on the interpretative sketch map. The locations of wells used in this study are shown on all maps. BFN = Brynhild Fault North; BFS = Brynhild Fault South; GF = Gudrun Fault.

(Sleipner Fm); SU2 = Early Callovian (Hugin Fm); SU3 = late Early Callovian–Late Oxfordian (Heather Fm); and SU4 = Late Oxfordian–Middle Volgian (lower Draupne Fm) (Fig. 2). Seven additional key stratal surfaces (e.g. flooding surfaces, unconformities, depositional hiatuses) are identified in wells and allow the four main syn-rift stratal units to be subdivided (Fig. 2).

4. Structural style

Within the study area two main Middle to Upper Jurassic rift-related normal faults are developed; the Gudrun and Brynhild Faults (Figs. 1b, c, 3b and 4). The structural style of these faults and associated (secondary) structures are described here.

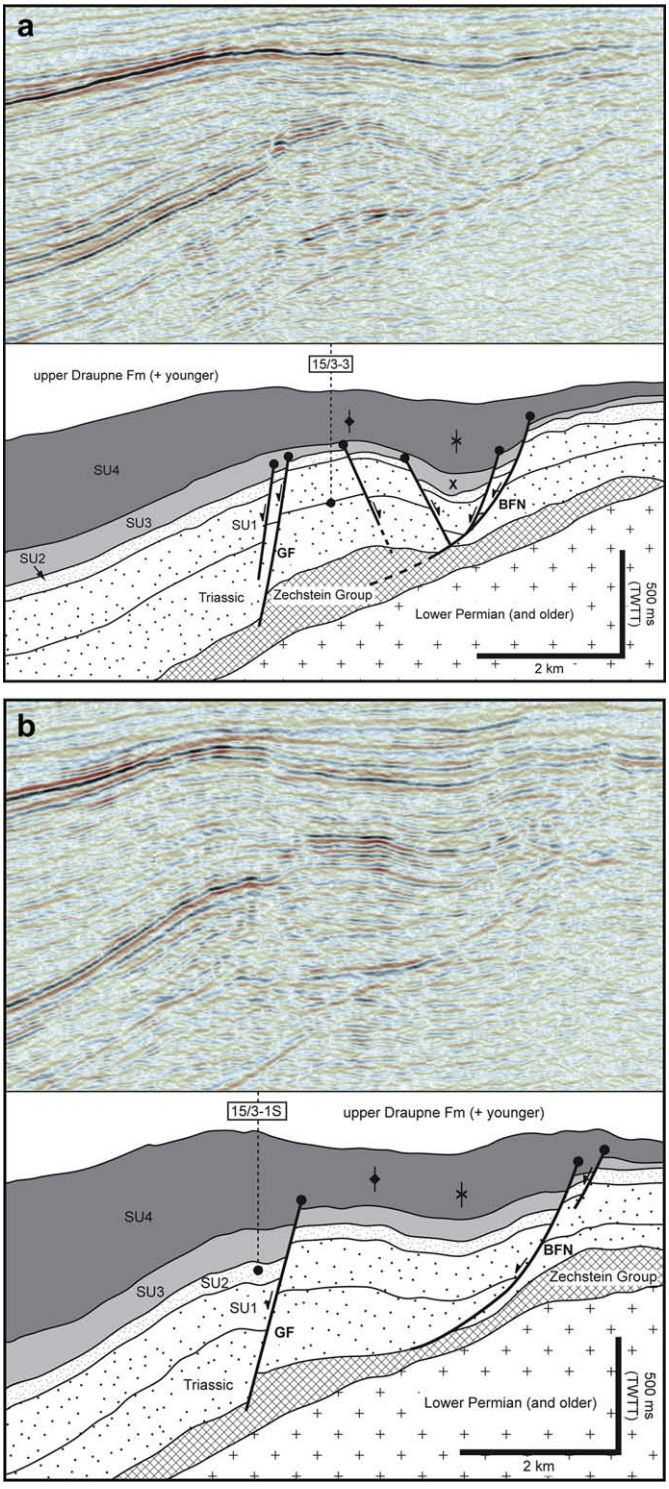

Fig. 4. Seismic cross-sections and corresponding geoseismic sections across the northern (a), central (b) and southern (c) parts of the study area. These illustrate the dip geometry and spatial relationship between the Gudrun and Brynhild Faults and associated (secondary) structures. The mapped stratal units (SU) are indicated. Abbreviations for the key structures are the same as in Fig. 3. Note the development of low-relief anticlines in the immediate hangingwalls of the Gudrun and Brynhild faults; these are related to a post-rift inversion event which occurred during the latest Jurassic-Early Cretaceous. The locations of the seismic sections are shown on the top Hugin Fm time-structure map shown in Fig. 3b.

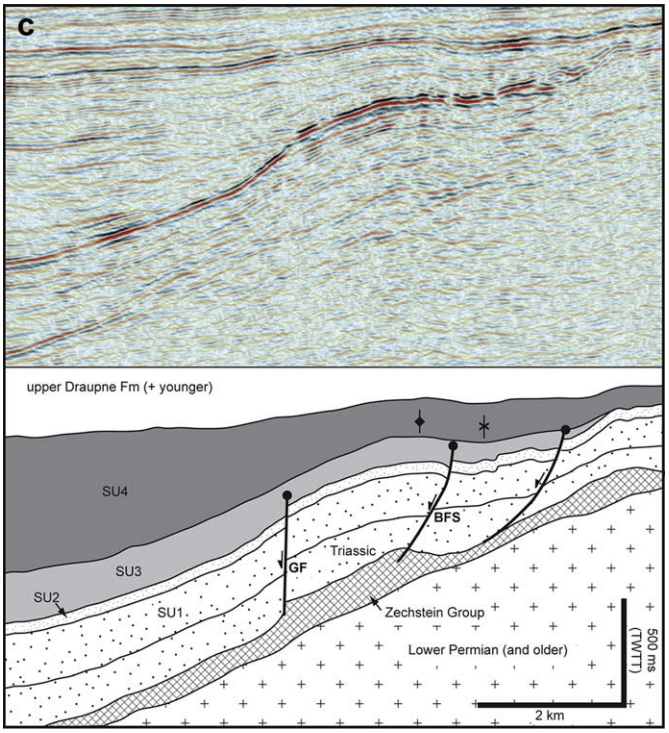

Fig. 4. (*continued*).

4.1. The Gudrun Fault

The Gudrun Fault strikes NE–SW and is 17 km in length. On time-migrated data the fault appears planar in cross-section and dips steeply towards the NW. The fault has a maximum throw of 272 ms (400–490 m) at its centre (Figs. 3b and 4). Where throw is greatest, the fault tips-out downwards at a steep angle into the upper part of the Zechstein Group and upwards into the lower part of SU4 (Fig. 4b). The fault-parallel anticline in the hangingwall of the Gudrun Fault is related to the latest Jurassic–Early Cretaceous inversion event and is not a rift-related structure (Fig. 4a and b) (Thomas and Coward, 1996; Jackson and Larsen, 2008). Apart from this later-formed structure, the Gudrun Fault is not associated with any rift-related deformation along the majority of its footwall or hangingwall. A series of normal faults with up to 50 ms (75–90 m) of throw are developed towards the northern tip of the fault. These structures splay-off into the footwall of the Gudrun Fault and tip-out 4.5 km along strike to the NE (Figs. 3b and 4a).

4.2. The Brynhild Fault

The Brynhild Fault is located to the SE of the Gudrun Fault, 5 km further up the hangingwall of the South Viking Graben; only a portion of the structure is located within the seismic dataset (Figs. 1a and 3b). The Brynhild Fault is at least 15 km long and can be divided into two geometrically separate segments; a southern segment which strikes NNE–SSW and dips towards the WNW, and a northern segment which strikes NE–SW and dips towards the NW (Figs. 3b and 4). The two fault segments are separated by an ENE–WSW-trending, NNW-dipping, 2 km wide relay ramp (Fig. 3b). On these time-migrated data both segments of the Brynhild Fault are strongly listric in cross-section. The faults shallow downwards into the upper part of the Zechstein Group, and steepen upwards into and tip-out within the middle part of SU4 (Fig. 4). Within the study area, the northern segment of the

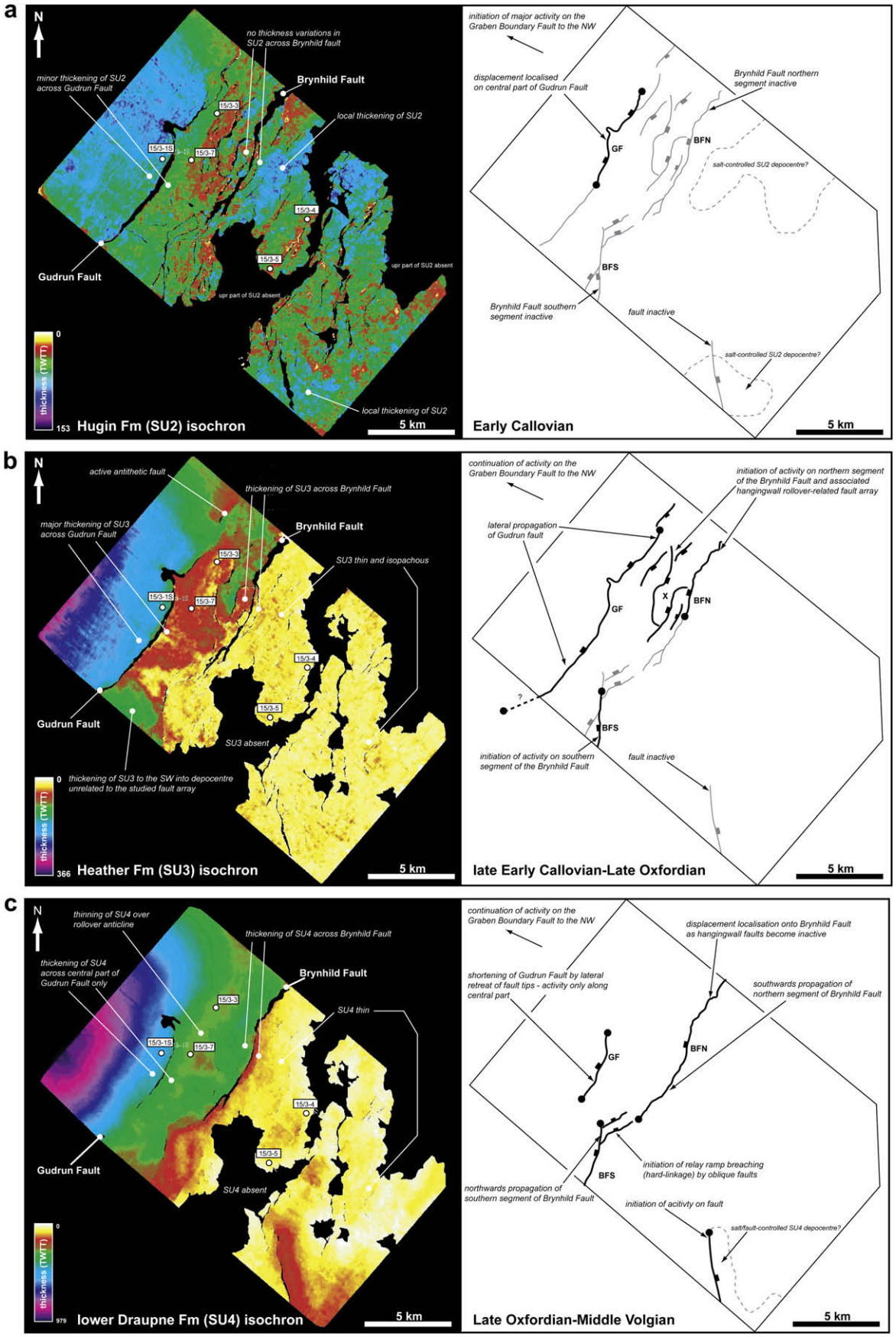
a
N
no thickness variations in SU2 across Brynhild fault
minor thickening of SU2 across Gudrun Fault
Brynhild Fault
local thickening of SU2
15/3-3
15/3-1S
15/3-7
15/3-4
15/3-5
upr part of SU2 absent
upr part of SU2 absent
Gudrun Fault
0
thickness (TWTT)
153
Hugin Fm (SU2) isochron
5 km
initiation of major activity on the Graben Boundary Fault to the NW
displacement localised on central part of Gudrun Fault
Brynhild Fault northern segment inactive
GF
BFN
salt-controlled SU2 depocentre?
BFS
Brynhild Fault southern segment inactive
fault inactive
salt-controlled SU2 depocentre?
Early Callovian
5 km
b
N
active antithetic fault
thickening of SU3 across Brynhild Fault
major thickening of SU3 across Gudrun Fault
Brynhild Fault
SU3 thin and isopachous
15/3-3
15/3-1S
15/3-7
15/3-4
15/3-5
Gudrun Fault
SU3 absent
0
thickness (TWTT)
thickening of SU3 to the SW into depocentre unrelated to the studied fault array
366
Heather Fm (SU3) isochron
5 km
continuation of activity on the Graben Boundary Fault to the NW
initiation of activity on northern segment of the Brynhild Fault and associated hangingwall rollover-related fault array
lateral propagation of Gudrun fault
GF
BFN
BFS
initiation of activity on southern segment of the Brynhild Fault
fault inactive
late Early Callovian-Late Oxfordian
5 km
c
N
thinning of SU4 over rollover anticline
thickening of SU4 across Brynhild Fault
thickening of SU4 across central part of Gudrun Fault only
Brynhild Fault
SU4 thin
15/3-3
15/3-1S
15/3-7
15/3-4
15/3-5
Gudrun Fault
SU4 absent
0
thickness (TWTT)
979
lower Draupne Fm (SU4) isochron
5 km
continuation of activity on the Graben Boundary Fault to the NW
displacement localisation onto Brynhild Fault as hangingwall faults become inactive
shortening of Gudrun Fault by lateral retreat of fault tips - activity only along central part
southwards propagation of northern segment of Brynhild Fault
GF
BFN
BFS
initiation of relay ramp breaching (hard-linkage) by oblique faults
northwards propagation of southern segment of Brynhild Fault
initiation of acitivty on fault
salt/fault-controlled SU4 depocentre?
Late Oxfordian-Middle Volgian
5 km

Brynhild Fault has a maximum throw of 495 ms (730–890 m) and the southern segment has a maximum throw of 50 ms (75–90 m).

In contrast to the Gudrun Fault, the hangingwall of the Brynhild Fault is deformed by a variety of structures. Firstly, an anticline and a syncline are developed, both of which trend parallel to the local strike of the adjacent fault segments (Figs. 3b and 4). Both the anticlines and synclines are symmetrical, open and have gently dipping limbs. The folds die-out along strike which corresponds to an along strike decrease in throw on the component segments of the Brynhild Fault (Fig. 3b). The fault-parallel folds are deformed by numerous moderate throw (up to 200 ms or 295–360 m) faults. These strike parallel to (NE–SW) and are either synthetic (i.e. NW-dipping) or antithetic (i.e. SE-dipping) to the main structure. The faults tip-out downwards into the Zechstein Group or link with the Brynhild Fault at-depth, and tip-out upwards into the middle to upper part of SU3 or the lower part of SU4 (Figs. 3b and 4a).

4.3. General model for the evolution of the hangingwall fault array

Although differing in terms of their cross-sectional geometry and total throw, both the Gudrun and Brynhild Faults dip towards the NW–WNW and detach downwards onto or into evaporite-rich units of the Zechstein Group (Fig. 4). Based on 2D seismic data, Thomas and Coward (1996) made similar observations and noted that deformation in the supra-Zechstein succession was decoupled from sub-evaporite, basement-involved faulting. Based on these observations, Thomas and Coward (1996) interpreted that the initiation of activity on the Gudrun and Brynhild Faults was triggered during the Late Callovian by the initiation of activity on the Graben Boundary Fault Zone, W to WNW-tilting of the South Viking Graben and gravity-induced gliding and extensional faulting of supra-Zechstein units. We follow this general interpretation for the origin of the Gudrun and Brynhild Faults, and in the following sections build on it by investigating the temporal and spatial evolution of these structures in greater detail.

5. Syn-rift stratal architecture and temporal evolution of the fault array

The evolution of normal faults impacts basin morphology and the generation of accommodation. Therefore, the architecture of coeval syn-rift stratal units has the potential to provide a record of fault zone and fault array evolution (e.g. Schlische and Anders, 1996; Cowie et al., 2000, 2007; McLeod et al., 2000; Sharp et al., 2000; Young et al., 2001; Gawthorpe et al., 2003). Specifically, thickness variations and the spatial development of key stratal surfaces within syn-rift units may directly reflect variations in syn-depositional, fault-driven subsidence and uplift. Based on these criteria, the aim of this section is to use both 3D seismic and well data to analyse depositional patterns in the syn-rift succession to provide temporal and spatial constraints on the evolution of the studied fault array (cf. methodologies of McLeod et al., 2000; Young et al., 2001). A two-fold approach is utilised here; this includes the interpretation of 3D seismic data and construction of seismic isochron (thickness) maps of syn-rift stratal units (Fig. 5), and the correlation of these units in wells (Fig. 6). Both these methods allow thickness variations to be determined and syn-depositional fault activity to be inferred. Importantly, in some cases, well data provide a higher temporal resolution of fault activity than that afforded by seismic data alone. There is some uncertainty in stratal thicknesses defined by seismic data due to limitations in the vertical resolution of these data. In particular, caution should be exercised when interpreting thickness patterns where the observed thicknesses are at or less than that of the interpreted vertical resolution (i.e. 30 m or 18 ms TWT). However, in most cases presented here, stratal thicknesses are typically significantly above this value, especially adjacent to the studied structures.

Before this analysis is presented, it should be noted that spatial variations in sediment thickness are used in this study as a *proxy* for spatial variations in subsidence, and not as a *direct* (quantitative) measure of subsidence. This is because a quantitative link between preserved stratal thickness and actual subsidence depends on variables such as water depth, sedimentation rate, depositional regime and compaction. All of these parameters are difficult to quantify and are likely to vary markedly through time (see discussions by McLeod et al., 2000; Young et al., 2001; Childs et al., 2003; Taylor et al., 2008). With respect to this study, it is assumed that accommodation developed due to fault slip was rapidly (on a geological timescale) filled with sediment, such that little or no topography developed at the seabed. In addition, it is interpreted that there was minimal erosion of fault hangingwalls or footwalls by sedimentary processes such as gravity flow-related erosion or fault-scarp degradation. These assumptions are considered reasonable given that: (i) there is no seismic evidence for degradation of the fault scarps (Fig. 4); and (ii) although gravity-flow deposits are identified in the syn-rift stratigraphy (see Fraser et al., 2003), bio-stratigraphically-constrained stratal surfaces can be identified in both footwall and hangingwall locations (e.g. in SU2 and 3 between wells 15/3-1S and 3-7; Fig. 6) . This suggests that the basin was overfilled for much of the period of interest and that topography did not develop at the seabed. A number of unconformities are identified within the syn-rift succession that document minor erosional and/or depositional hiatuses (condensation) (Fig. 6). These are developed either in the footwalls to Late Jurassic faults (i.e. top SU3 unconformity in 15/3-7 and 3-3 in the footwall of the Gudrun Fault; Fig. 6) or towards the basin margin (i.e. the unconformities bounding SU3 in 15/3-4 and 3-5; Fig. 6). The observation that; (i) these unconformities are generally better-developed and of longer duration towards the basin margin, and (ii) erosion associated with these surfaces is never greater in the hangingwalls than the footwalls of the studied faults, suggest that these surfaces do not markedly modify the tectonically-controlled, bulk thickness variations within the syn-rift stratal units. Therefore, these unconformities are interpreted not to adversely affect this analysis.

5.1. Stratal Unit 1 (Early Bathonian–Late Bathonian)

5.1.1. Description

Stratal Unit 1 is Early Bathonian–Late Bathonian in age and corresponds lithostratigraphically to the Sleipner Formation (SU1; Fig. 2). On seismic data, due to poor resolution at-depth, it is not possible to confidently map the top, base, and hence total thickness of SU1 over much of the study area. Where data quality is best, seismic data indicate that SU1 displays no thickness variation across the Gudrun Fault and thickens downdip to the NW towards the Graben Boundary Fault Zone (Fig. 4). Although imaging is poorer adjacent to and immediately updip of the Brynhild Fault, seismic data suggest that SU1, and the underlying Triassic units to

Fig. 5. Seismic isochron (thickness) maps of the main syn-rift stratal units (SU). Sequential map-view reconstructions for each time interval illustrating the inferred fault activity and, where interpreted, halokinesis; these are based on the thickness trends observed on seismic and well data (see Fig. 6). (a) SU2 (Hugin Fm; Early Callovian); (b) SU3 (Heather Fm; late Early Callovian–Late Oxfordian); (c) SU4 (lower Draupne Fm; Late Oxfordian–Middle Volgian). Abbreviations for the key structures are the same as in Fig. 3. See text for full discussion.

Fig. 6. Stratigraphic correlation of key wells within the study area illustrating thickness variations in the studied syn-rift stratal units (SU). The tectono-stratigraphic significance of the various syn-rift stratal units is indicated in the column of the left-hand side, as are the identified stratal sub-units (A, B, C, etc). The line of section is shown on the inset map; this is a simplified syn-rift structure map based on the top-SU2 (top Hugin Fm) time-structure map (see Fig. 3B). Thick solid black lines represent regionally mappable, stratal unit-bounding surfaces; thin dashed lines represent locally identified stratal surfaces which define sub-units; very thick black lines represent unconformities. GR = Gamma-ray. Note the thickening of SU1 (Sleipner Fm) and SU2 (Hugin Fm) across the Brynhild Fault is apparent, and is related to overall NW-thickening of these units rather than abrupt thickening across the fault.

an even greater degree, thin towards the northern segment of this structure and continue to thin south-eastwards across a low-relief evaporite pillow located 1.5 km into its footwall (Fig. 4).

SU1 is fully penetrated in two of the five wells where it unconformably overlies the Skagerrak Formation and is conformably overlain by SU2 (Fig. 6). Due to its terrestrial character, detailed biostratigraphic data within SU1 is not available, thus it is not possible to comprehensively evaluate the detailed internal stratigraphic architecture of this unit. In general, however, it is observed that the unit thickens towards the NW (Fig. 6); this observation is consistent with seismic observations to the NW of the Gudrun Fault which also indicate north-westwards thickening (Fig. 4).

5.1.2. Interpretation of Early Bathonian–Late Bathonian tectonics

The absence of thickness variations in SU1 suggest this unit was deposited prior to the initiation of activity on the main faults within the study area. Thickening towards the NW indicates that the Graben Boundary Fault Zone was active at this time, however. Local thickness variations in SU1 and Triassic units immediately SE of the Brynhild Fault indicate a period of Zechstein Group halokinesis during the Triassic to Middle Jurassic, formation of a low-relief pillow in this location prior to the main rift episode (Fig. 7a).

5.2. Stratal Unit 2 (Early Callovian)

Description. Stratal Unit 2 is Early Callovian in age and corresponds lithostratigraphically to the Hugin Formation (SU2; Fig. 2). On seismic data SU2 thickens north-westwards across the central part of the Gudrun Fault and further downdip to the NW into the axis of the South Viking Graben (Figs. 4 and 5a). Seismic sections indicate that despite thickening across the Gudrun Fault, SU2 is not wedge-shaped and does not diverge into the hangingwall of the fault (Fig. 4). Up the hangingwall further to the SE, SU2 does not thicken across the Brynhild Fault despite this structure having several hundreds of metres of throw present-day (Figs. 4 and 5a). In addition to thickness variations directly related to the Gudrun Fault, local depocentres (blue areas in Fig. 5) are observed in SU2 which do not appear to be directly related to normal faults. For example, in the footwall of the Brynhild Fault, a NE–SW-trending depocentre is developed, in addition to a series of sub-circular depocentres located 2.5 km to the ENE of well 15/3-4 and 7.5 km to the SSE of well 15/3-5 (Fig. 5). The thickness of SU2 appears to be inversely related to the thickness of the underlying Zechstein Group; thicker areas of SU2 occur above areas where the Zechstein Group is thin and vice-versa (cf. Figs. 3b and 5). Across the crests of salt-cored structural highs SU2 may be very thin or absent (see Figs. 1b and 3b).

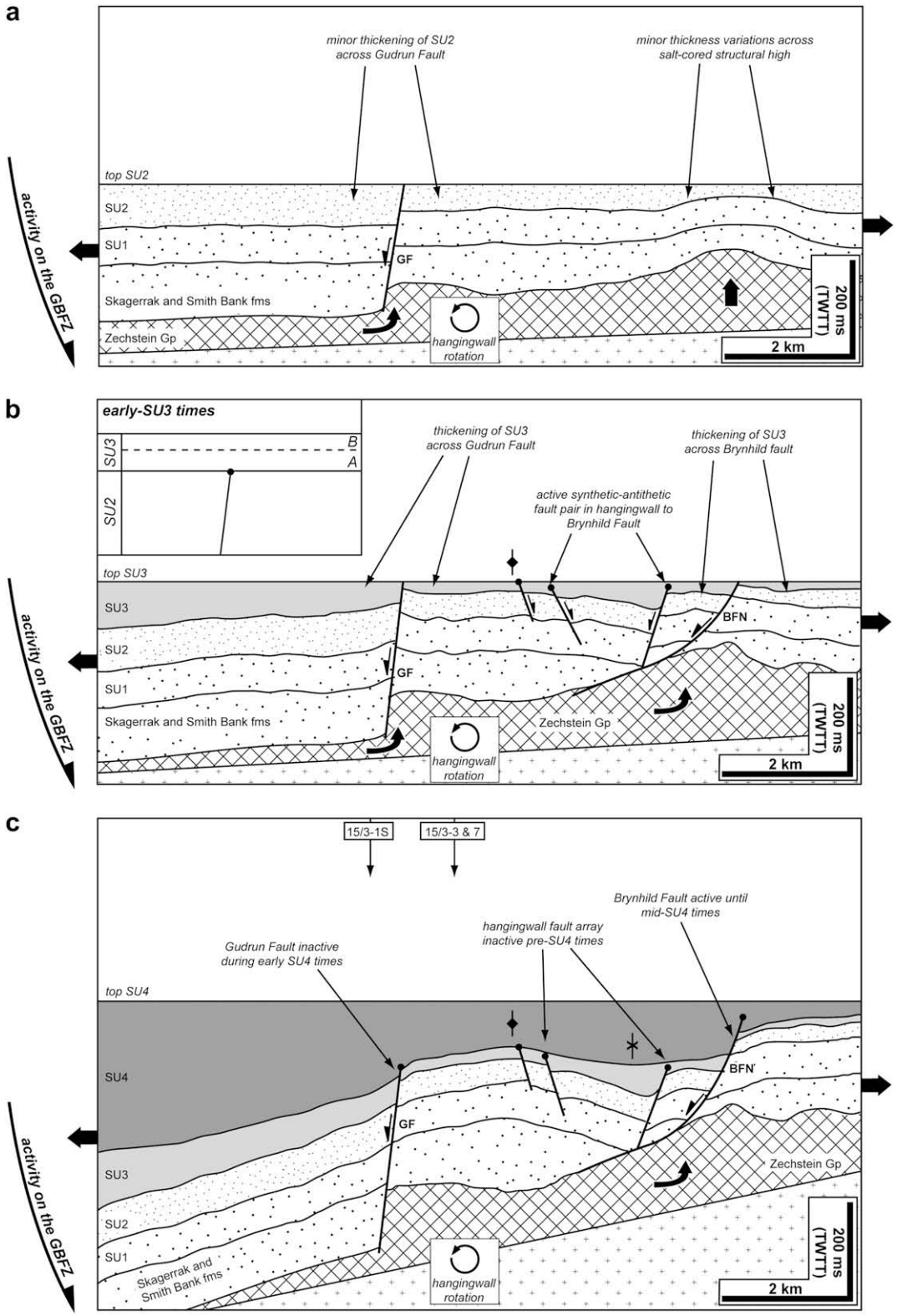

Fig. 7. Sequential cross-sections across the study area illustrating the temporal and spatial development of the studied fault array. Although schematic, these cross-sections are broadly based on a sequentially flattened seismic section taken through the centre of the study area (see line X-X' on interpretative map shown in Fig. 3b). (a) SU2 (Hugin Fm; Early Callovian); (b) SU3 (Heather Fm; late Early Callovian–Late Oxfordian); the inset shows an illustration of early-SU3 times when the Gudrun Fault is interpreted to have been temporarily inactive based on well data (see Fig. 6 and discussion in text); (c) SU4 (lower Draupne Fm; late Oxfordian–Middle Volgian). Thick black arrows within the Zechstein Group in all figures indicate inferred direction of salt movement. In (c), wells 15/3-1S, 3-3 and 3-7 are projected onto the line of section such that the final reconstructed geometry can be compared to actual well data (see Fig. 6). Abbreviations for the key structures are the same as in Fig. 3. Black arrows within the Zechstein group indicate the main directions of salt movement in 2D.

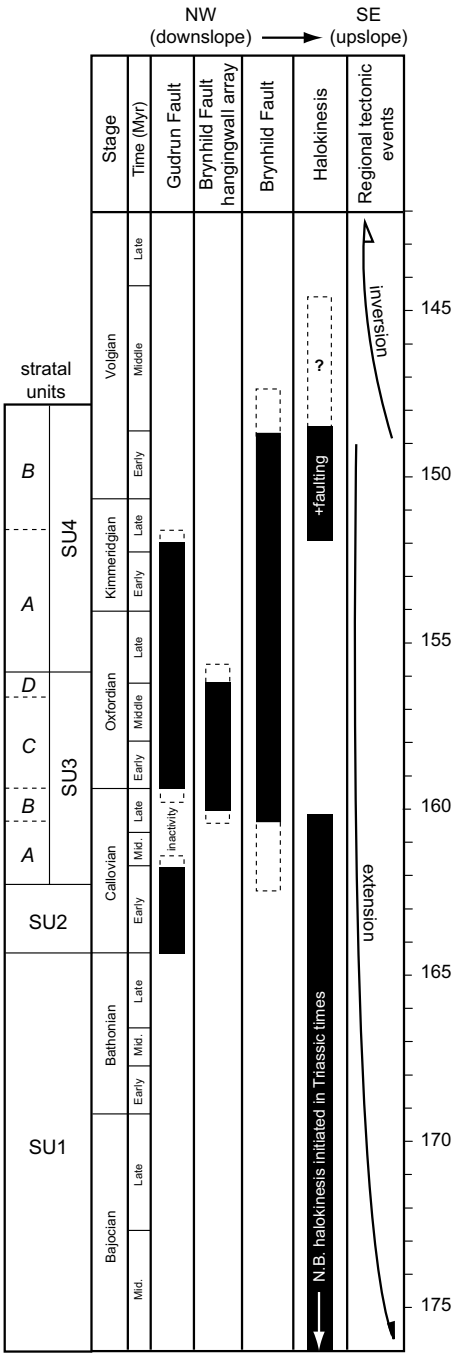

Fig. 8. Simplified fault activity diagram illustrating the temporal and spatial evolution of the studied fault array. Solid black boxes indicate the duration of activity for each of the major studied structures (Gudrun and Brynhild Fault). Dashed box outlines schematically illustrate some of the uncertainties on the timing of initiation and cessation of fault activity (for example where a 'Late Kimmeridgian' or late Early Callovian' age is given). Periods of halokinesis and the activity of faults located in the hangingwall of the Brynhild Fault are also indicated. Note the overall upslope (south-eastwards) migration of active faulting through time.

Except for one well located in the hangingwall of the Gudrun Fault, SU2 is fully penetrated in all wells (Fig. 6). SU2 conformably overlies SU1 across much of the study area and is itself either conformably or unconformably overlain by SU3. In the centre of the footwall of the Gudrun Fault, SU2 is 213.7 m thick (i.e. 15/3-7; Fig. 6). Although the base of SU2 is not penetrated in the hangingwall of the Gudrun Fault (i.e. 15/3-1S; Fig. 6), based on the seismically-measured 'thickness' of the unit it is calculated that it is *ca.* 360 m thick; this indicates thickening of SU1 across the central part of the Gudrun Fault which is consistent with seismic evidence (cf. Figs. 5a and 6). Importantly, despite thinning across the Gudrun Fault, the four sub-units within SU2 can be identified on both sides of the fault (Fig. 6). This indicates that little or no footwall erosion took place during deposition of this unit and that the basin was, at least locally, overfilled (see discussion above). Up the hangingwall towards the SE, SU2 thins, with thinning appearing to be partly related to erosion of the upper part of the unit beneath a late Early Callovian unconformity at the base of SU3 (Fig. 6).

5.2.1. Interpretation of Early Callovian tectonics

Expansion of SU2 towards the NW indicates ongoing activity on the Graben Boundary Fault Zone. In addition, local thickening of SU2 across the Gudrun Fault indicates that this structure became active at this time (Figs. 5a, 7a and 8). As discussed above, activity on the Gudrun Fault was triggered by the initiation of major activity on the Graben Boundary Fault Zone, westward tilting of the hangingwall, and extension of Triassic to lower Middle Jurassic units above the Zechstein Group (Fig. 7a). Seismic data suggest that only a 7 km long portion towards the northern end of the Gudrun Fault was active at this time (Fig. 5a), compared to the present fault length of 17 km. Subsidence in the hangingwall of the Gudrun Fault would have required thinning of the Zechstein Group evaporites. This could have been accommodated by migration of the evaporites updip to the E into the low-relief pillow observed in the footwall of the fault, into larger structures located further updip to the SE or downdip to the NW towards the axis of the South Viking Graben (Fig. 7a), or laterally along strike of the Gudrun Fault towards its tips (cf. Petersen et al., 1992; Thomas and Coward, 1996; Harvey and Stewart, 1998).

Although the Gudrun Fault had become active during this time, the Brynhild Fault was still inactive (Figs. 5a, 7a and 8). Thickness variations in SU2 which are not related to Late Jurassic faults may reflect differential subsidence related to halokinesis of the Zechstein Group. This interpretation is supported by the observation that SU2 is thickest where the top of the Zechstein Group is structurally lowest (see Fig. 1b and compare Figs. 3a and 5a), suggesting that withdrawal of the Zechstein Group led to syn-depositional subsidence. Halokinesis may have been triggered by differential loading of shallow marine deposits (i.e. Hugin Fm) above the evaporite layer (Fig. 7a).

5.3. Stratal Unit 3 (late Early Callovian–Late Oxfordian)

5.3.1. Description

Stratal Unit 3 is late Early Callovian–Late Oxfordian in age and corresponds lithostratigraphically to the Heather Formation (SU3; Fig. 2). Although seismic data indicate that SU3 thickens towards the NW (Figs. 4 and 5b), SU3 displays markedly different local thickness variations to that observed in underlying stratal units. Firstly, SU3 thickens across the entire length of the Gudrun Fault in contrast to SU2 which only thickened across a 7 km long portion of the fault (Fig. 5b). As observed for SU2, SU3 is tabular within and does not diverge towards the hangingwall of this fault. Secondly, SU3 thickens across both the northern 5.7 km of the northern segment of the Brynhild Fault, and the southern 4 km of the southern segment of this fault; SU2 displayed no thickness variations with respect any part of this structure (cf. Fig. 5a and b). In cross-section, SU3 is wedge-shaped within and diverges towards the hangingwall of the Brynhild Fault (Fig. 4a). Finally, SU3 thickens across several of the low-throw faults located in the hangingwall of the Brynhild Fault (Figs. 4a and 5b). This is particularly well-illustrated in association with a synthetic-antithetic fault pair which bound a 1.4 km wide graben (labelled X in Figs. 4 and 5b) located 1.8 km into the hangingwall of the

fault. SE of the Brynhild Fault, further up the hangingwall, SU3 is thin and displays no thickness variations adjacent to evaporite-cored structural highs (Figs. 4 and 5b).

SU3 is penetrated by all wells within the study area. In the W the unit conformably overlies SU2, whereas in the east this lower contact is unconformable (Fig. 6). SU3 is unconformably overlain by SU4, except in the immediate hangingwall of the Gudrun Fault where this contact is conformable (Fig. 6). Internally, SU3 can be subdivided into four sub-units based on the identification of three age-constrained flooding surfaces (Figs. 2 and 6). SU3 thickens north-westwards across the Gudrun Fault, although correlation of the four internal sub-units reveals that thickening is not equally distributed within the unit. The lower two, Callovian sub-units are of equal thickness either side of the fault, whereas both the upper two, Oxfordian sub-units more than double in thickness into the hangingwall of the fault (compare sub-units A and B with C and D; Fig. 6). In addition to these local thickness variations, SU3 thins towards the SE up the hangingwall, where the unit is bound below and above by Late Callovian and Late Oxfordian unconformities respectively (Fig. 6). Despite being thin and bounded by unconformities in the SE, the upper two flooding surfaces within SU3 can still be identified. In contrast, the lowermost flooding surface is absent and is interpreted to have merged with the Late Callovian unconformity which bounds the base of the unit (Fig. 6).

5.3.2. Interpretation of late Early Callovian–Late Oxfordian tectonics

Thickening of SU3 to the NW reflects ongoing activity on the Graben Boundary Fault Zone (Fig. 5). Continued growth of the Gudrun Fault is interpreted to reflect ongoing activity on the Graben Boundary Fault Zone and associated hangingwall tilting (Figs. 7b and 8). Thickening of SU3 along the entire mapped length of the Gudrun Fault indicates that the fault had increased in length by *ca*. 10 km from SU2 times (cf. Fig. 5a and b), with mostly propagation towards the S and only minor propagation towards the N (cf. Fig. 5a and b). Importantly, well data suggest that growth of the Gudrun Fault was not constant during this time. Restriction of thickness variations to the upper, Oxfordian part of SU3 (i.e. Fig. 6) suggests a *ca*. 2.8 Myr period of relative inactivity on the Gudrun Fault during the Middle to Late Callovian (see inset in Figs. 7b and 8).

Continued activity on the Gudrun Fault during SU2 times is interpreted to have resulted in 'unbuttressing' of the supra-Zechstein Group units updip to the SE. This led to gravity-induced sliding of supra-Zechstein Group units on this detachment and formation of the Brynhild Fault (Figs. 7b and 8). An alternative interpretation is that the Brynhild Fault and associated structures formed solely due to salt withdrawal related to continued growth of pre-existing salt pillows located to the SE and to the NW. However, major expansion of SU4 to the NW (Fig. 4) and regional observations (see Fraser et al., 2003) indicate that the Graben Boundary Fault Zone was very active at this time, suggesting that continued hangingwall rotation was the most likely control on the formation of the Brynhild Fault and associated structures. Isochron data indicate that only the northernmost part of the northern segment, and southernmost part of the southern segment, were active at this time (Fig. 5b). Due to a lack of well data immediately adjacent to the Brynhild Fault, it is difficult to further constrain the suggested late 'Early Callovian to Late Oxfordian' initiation age for this structure. It may be speculated that the Brynhild Fault became active during the Early Oxfordian in response to the major period of activity identified on the Gudrun Fault to the NW.

The listric geometry of the Brynhild Fault led to the formation of a rollover anticline and associated faults in its hangingwall (Figs. 7b and 8). These formed to accommodate strain associated with hangingwall folding (e.g. Gibbs, 1984; McClay, 1990; Roberts and Yielding, 1994). It is interpreted that the majority of these faults were active during the latest Callovian to Early Oxfordian (Fig. 8) as they mainly accommodate thickness changes in the lower part of SU3 and only locally offset the top of this unit (Figs. 4a and inset in Fig. 7b). Finally, in contrast to SU1 and SU2 times, halokinesis updip to the SE of the Brynhild Fault is not apparent at this time (Fig. 5b).

5.4. Stratal Unit 4 (Late Oxfordian–Early Volgian)

5.4.1. Description

Stratal Unit 4 is Late Oxfordian–Early Volgian in age and corresponds lithostratigraphically to the lower part of the Draupne Formation (SU4; Fig. 2). Seismic data demonstrate that although thickening overall towards the NW, SU4 displays markedly different local thickness variations to those observed in the underlying stratal units. Firstly, SU4 only thickens across a 5.5 km long, central portion of the Gudrun Fault (Fig. 5c). Thickening only occurs in the lower part of the unit, with the fault tipping out upwards within the middle part of the unit (Fig. 4b). Secondly, SU4 thickens along the entire length of the northern and southern segments of the Brynhild Fault, and has a wedge-shaped geometry within and diverges towards the hangingwall of these structures (Figs. 4 and 5a). Finally, subtle thickening of SU4 is observed across two NW-dipping faults located in a relay ramp between the northern and southern segments of the Brynhild Fault (Fig. 5c). SU4 is thinner overall to the SE of the Brynhild Fault, although thickening of the unit into a fault-bounded basin is observed (indicated in Fig. 5c). Additional subtle thickness variations in SU4 in the SE of the study area are related to the magnitude of erosion at the top of the unit beneath the Base Cretaceous Unconformity.

SU4 is fully penetrated by all wells. The contact of SU4 with SU3 is unconformable across the study area, except in the immediate hangingwall of the Gudrun Fault where this contact is conformable (Fig. 6). The contact of SU4 with overlying stratal units is conformable across the study area (Fig. 6). In the western part of the study area, SU4 can be sub-divided into two sub-units (A and B; Fig. 6) based on the identification of a Late Kimmeridgian flooding surface. It is noted that this surface is not offset across the Gudrun Fault but is offset across the Brynhild Fault (Fig. 6). Upward tip-out of the Gudrun Fault indicates that thickening across this structure is accommodated solely by the lower (Late Oxfordian–Late Kimmeridgian) sub-unit of SU4. In contrast, the upper (Late Kimmeridgian–Middle Volgian) sub-unit is broadly tabular across this fault (cf. sub-units A and B; Fig. 6).

5.4.2. Interpretation of Late Oxfordian–Early Volgian tectonics

Thickening of SU4 towards the NW indicates ongoing activity on the Graben Boundary Fault Zone at this time (Fig. 7c). The absence of thickening of the SU4 across much of the Gudrun Fault suggests that this structure had shortened via lateral retreat of its tips and become inactive along much of its length (Fig. 5c). In addition, well data indicate that the Gudrun Fault was active during the Early to early Late Kimmeridgian (i.e. sub-unit A times; Figs. 6–8), but became inactive during the Late Kimmeridgian (i.e. sub-unit B times; Figs. 6–8).

The Brynhild Fault continued to grow via lateral propagation of its tips, with the southern tip of the northern segment propagating at least 5 km to the SW, and the northern tip of the southern segment propagating 0.9 km to the NE (Fig. 5c). Propagation of the two fault segments towards each other and eventual overlap of their tips resulted in the formation of a 2-km wide, NNW-dipping relay ramp (Fig. 5c). The two ENE–WSW striking faults developed within the relay ramp became active at this time, and are interpreted to have formed during the early stages of hard-linkage (*sensu* Peacock and Sanderson, 1994) of the two segments of the

Brynhild Fault . Upward tip-out of the majority of the Brynhild Fault hangingwall faults in the upper part of SU3 indicates death of these faults prior to SU4 times (Figs. 7c and 8). The cessation of activity on these structures appears to coincide with the southwards propagation of the northern segment of the Brynhild Fault, suggesting strain had now become localised on the larger structure (Figs. 5c and 7c). The Brynhild Fault became inactive during the Early to Middle Volgian as indicated by the upward tip-out of the Brynhild Fault into the middle part of SU4 (Figs. 7c and 8). Ongoing activity on the Graben Boundary Fault Zone and westwards rotation of the hangingwall resulted in continued updip migration of deformation as indicated by the initiation of faulting 10 km SE of the Brynhild Fault (Fig. 5c).

All faults within the study area became inactive during the latest Jurassic; this coincides with the end of the main extensional episode and a change to a compressional regime characterised by inversion (Fig. 8) (Pegrum and Ljones, 1984; Cherry, 1993; Thomas and Coward, 1996; Branter, 2003; Fletcher, 2003a,b; Jackson and Larsen, 2008).

6. Discussion and conclusions

6.1. Gravity-driven fault array development above a mobile detachment

Rift-related, gravity-driven normal fault arrays developed above evaporite-rich detachments have previously been described from subsurface analysis of several locations on the UK continental shelf (i.e. East Central Graben and Irish Sea Basin; Penge et al., 1993, 1999; the Forties–Montrose High; Clark et al., 1993; the Renee Ridge; Clark et al., 1998; Durward–Dauntless area; Stewart et al., 1999; the Puffin High; Davies et al., 2001). In these examples, the initiation of faulting coincided with the main period of Late Jurassic rifting and half-graben rotation, and evaporite-dominated units of the Upper Permian Zechstein Group acted as the intra-stratal detachment. Penge et al. (1993, 1999) used the term '*rift–raft tectonics*' to describe the kinematic linkage between rifting and thin-skinned extension above an intra-stratal detachment. Gravity-driven deformation with a similar overall structural style has also been described from several passive margins (e.g. offshore Angola; Duval et al., 1992; Spathopolous, 1996; offshore Brazil; Demercian et al., 1993; Cobbold et al., 1995; offshore Gabon; Gaullier et al., 1993). In these settings this style of deformation is termed '*raft tectonics*' and the causal mechanism for deformation is also related to basin tilting and thin-skinned extension above an intra-stratal detachment. On passive margins, however, basin tilting is associated with thermal subsidence and sediment loading, rather than normal faulting.

This study provides important insights into the kinematic and temporal development of gravity-driven fault arrays in rifts. It indicates that individual segments within the evolving fault array grew via fault-tip propagation and, in one example, shortened via tip retreat. In addition, fault growth is not synchronous, and marked diachroneity in the initiation, growth and decay of faults within the evolving array is observed (Fig. 8). More specifically, it is demonstrated that faulting migrates progressively updip with time (Fig. 8), in a manner similar to that described from subsurface studies of raft tectonics on passive margins (Duval et al., 1992; Spathopolous, 1996; Demercian et al., 1993; Gaullier et al., 1993; Cobbold et al., 1995; Imber et al., 2002) and from physical analogue models of gravity-driven fault growth (Childs et al., 1993). Systematic updip migration of active faulting through time reflects progressive 'unbuttressing' and associated faulting of upslope 'proto-rafts'. Whether the spatial evolution of gravity-driven fault arrays is common to systems in both rifts and on passive margins requires further analysis. It may be speculated that the temporal evolution of rift-related gravity-driven systems would be directly linked to the rate of slip on the basin-bounding fault and associated rate of hangingwall tilting. Likewise, in passive margin settings, the rate of fault migration would be related to both the rate of thermal subsidence and sediment loading.

Many of the new observations into the structural style and evolution of gravity-driven fault arrays presented in this study are a direct consequence of the data used. For example, previous studies have utilised widely-spaced 2D seismic data and have focused almost exclusively on describing the general structural style of the fault systems (Clark et al., 1993; Penge et al., 1993, 1999; Bishop et al., 1995; Thomas and Coward, 1996; Clark et al., 1998; Davies et al., 2001; but see Petersen et al., 1992 for an exception). With such datasets, it is difficult to unequivocally map the geometry and distribution of individual fault segments, the style of associated (secondary) deformation and thickness variations in syn-tectonic stratal units (see discussion by Cartwright and Huuse, 2005). Furthermore, in previous studies, detailed stratigraphic and biostratigraphic data have not been available and/or sufficiently integrated with the seismic observations to provide additional temporal constraints on the evolution of the fault array. Finally, this study highlights that careful analysis of the internal seismic-stratigraphic architecture of 'undeformed' raft blocks on good-quality, preferably 3D seismic data, is essential to identifying pre-rift periods of halokinesis.

6.2. Structural evolution of rift basins

Existing models for the structural development of rifts indicate that hangingwalls are structurally relatively simple, especially during the late syn-rift when fault activity becomes localised onto a few large-displacement, basin-bounding structures (the rift-climax phase; Prosser, 1993; Cowie, 1998; Cowie et al., 2000; Gawthorpe and Leeder, 2000). In contrast, this study indicates that the hangingwalls of rift basins may be structurally complex throughout the rift event. The occurrence and style of deformation is linked to the presence of an intra-stratal detachment horizon at-depth within the evolving half-graben.

The systematic migration of fault activity up the hangingwall away from the axis of the half-graben differs from stress interaction-related models of rift-related fault array development (e.g. Cowie, 1998; Cowie et al., 2000, 2007; Gawthorpe and Leeder, 2000). These models indicate that an early period of distributed deformation is succeeded by a period when strain becomes localised on a few large-displacement, basin-bounding structures (the rift-initiation to rift climax transition; Prosser, 1993; Cowie, 1998, Cowie et al., 2000; Gawthorpe and Leeder, 2000). The difference in the spatial development of the fault array is again linked to the fact that faulting is gravity-driven rather than related to true crustal extension. Therefore, care should be taken when applying generic tectono-stratigraphic models of rift evolution to basins were intra-stratal detachments are present within the evolving half-graben.

6.3. The Late Jurassic structural evolution of the South Viking Graben

Based on previous regional studies of the South Viking Graben, the significance of deformation described in this study can be placed in its basin-scale context. The initiation of thin-skinned extension in the study area is linked to hangingwall rotation associated with the initiation of movement on the Graben Boundary Fault Zone to the W. As this model requires tilting of the hangingwall to initiate thin-skinned extension, it is likely that

deformation within the study area occurred some time after the initiation of activity on the basin-bounding fault. Previous studies suggest that Late Jurassic activity on the Graben Boundary Fault Zone commenced in the Early to Late Callovian, with the main period of activity occurring in the Oxfordian (Cockings et al., 1992; Cherry, 1993; McClure and Brown, 1992; Fletcher, 2003a,b). The observation that activity on the hangingwall fault array commenced in the Early Callovian (Fig. 8) suggests that faulting was broadly synchronous across the basin. In addition, faulting on the hangingwall occurred after a relatively small amount of slip on the basin-bounding fault and, therefore, a relatively minor amount of hangingwall tilting. This interpretation is consistent with observations from physical analogue modelling (Childs et al., 1993; Gaullier et al., 1993) and structural restoration (Bishop et al., 1995) studies which suggest that gravity-induced sliding and associated faulting can occur after $<2^{\circ}$ of detachment tilting.

Acknowledgments

We would like to thank Karla Kane, Rachel Kieft, Anne Elise Tjemsland, Martha Withjack, Anna-Sofia Gregerson, Unni Stalsberg Sjursen, Sigmund Hanslien, Elisebeth Bjerkebeck and Helge Sognnes for discussions during the course of this study and StatoilHydro ASA for providing financial support. Journal reviewers Bruce Trudgill and Stefan Back are thanked for insightful and thorough reviews as is journal editor Joao Hippertt. Partners within licences PL303, 025 and 187 are thanked for permission to publish this study. The views expressed in this paper are the authors and do not necessarily represent those of StatoilHydro ASA or partners within the PL303 licence. Thanks also to Seismic Micro Technologies (Kingdom Suite) and Landmark (Seisworks and Stratworks) for access to software through provision of Academic Licence Agreements to Imperial College.

References

Anderson, J.E., Cartwright, J., Drysdall, S.J., Vivian, N., 2000. Controls on turbidite sand deposition during gravity-driven extension of a passive margin: examples from Miocene sediments in block 4, Angola. Marine and Petroleum Geology 17, 1165–1203.

Bishop, D.J., Buchanan, P.G., Bishop, C.J., 1995. Gravity-driven thin-skinned extension above Zechstein Group evaporites in the western central North Sea: an application of computer-aided restoration techniques. Marine and Petroleum Geology 12, 115–135.

Branter, S.R.F., 2003. The East Brae field, blocks 16/03a, 16/03b, UK North Sea. In: Gluyas, J.G., Hichens, H.M. (Eds.), United Kingdom Oil and Gas Fields, Commemorative Millennium Volume. Geological Society of London, Memoir, vol. 20, pp. 191–197.

Brehm, J., 2003. The North Brae and Beinn fields, blocks 16/7a, UK North Sea. In: Gluyas, J.G., Hichens, H.M. (Eds.), United Kingdom Oil and Gas Fields, Commemorative Millennium Volume. Geological Society of London, Memoir, vol. 20, pp. 199–209.

Cartwright, J.A., Huuse, M., 2005. 3D seismic technology: the geological 'Hubble'. Basin Research 17, 1–20.

Cherry, S.T.J., 1993. The interaction of structure and sedimentary process controlling deposition of the upper Jurassic Brae formation conglomerate, block 16/17, North Sea. In: Parker, J.R. (Ed.), Petroleum Geology of Northwest Europe: Proceedings of the Fourth Conference, pp. 387–400.

Childs, C., Easton, S.J., Vendeville, B.C., Jackson, M.P.A., Lin, S.T., Walsh, J.J., Watterson, J., 1993. Kinematic analysis of faults in a physical model of growth faulting above a viscous salt analogue. Tectonophysics 228, 313–329.

Childs, C., Nicol, A., Walsh, J.J., Watterson, J., 2003. The growth and propagation of synsedimentary faults. Journal of Structural Geology 25, 633–648.

Clark, D.N., Riley, L.A., Ainsworth, N.R., 1993. Stratigraphic, structural and depositional history of the Jurassic in the Fisher Bank Basin, UK North Sea. In: Parker, J.R. (Ed.), Petroleum Geology of Northwest Europe: Proceedings of the Fourth Conference, pp. 415–424.

Clark, J.A., Stewart, S.A., Cartwright, J.A., 1998. Evolution of the NW margin of the North Permian Basin, UK North Sea. Journal of the Geological Society of London 155, 663–676.

Cobbold, P.R., Szatmari, P., Demercian, L.S., Coelho, D., Rossello, E.A., 1995. Seismic and experimental evidence for thin-skinned horizontal shortening by convergent radial gliding on evaporites, deep-water Santos basin, Brazil. In: Jackson, M.P.A., Roberts, D.G., Snelson, S. (Eds.), Salt Tectonics: a Global Perspective. American Association of Petroleum Geologists Memoir, vol. 65, pp. 305–321.

Cockings, J.H., Gifford Kessler II, L., Mazza, T.A., Riley, L.A., 1992. Bathonian to mid-Oxfordian sequence stratigraphy of the South Viking Graben, North Sea. In: Hardman, R.F.P. (Ed.), Exploration Britain: Insights for the Next Decade. Geological Society, London, Special Publications, vol. 67, pp. 65–105.

Corredor, F., Shaw, J.H., Bilotti, F., 2005. Structural styles in the deep-water fold and thrust belts of the Niger Delta. Bulletin of the American Association of Petroleum Geologists 89, 735–780.

Coward, M.P., 1995. Structural and tectonic setting of the Permo–Triassic basins of northwest Europe. In: Boldy, S.A.R. (Ed.), Permian and Triassic Rifting in Northwest Europe. Geological Society, London, Special Publications, vol. 91, pp. 7–39.

Cowie, P.A., 1998. A healing-reloading feedback control on the growth rate of seismogenic fault. Journal of Structural Geology 20, 1075–1087.

Cowie, P.A., Gupta, S., Dawers, N.H., 2000. Implications of fault array evolution for synrift depocentre development: insights from a numerical fault growth model. Basin Research 12, 241–261.

Cowie, P.A., Roberts, G., Mortimer, E., 2007. Strain localisation with fault arrays over timescales of 10^0 to 10^7 years – observations, explanations and debates. In: Handy, M.R., Hirth, G., Hovius, N. (Eds.), Tectonic Faults: Agents of Change on a Dynamic Earth. MIT Press, Cambridge, MA Dahlem Workshop Report 95.

Damuth, J.E., 1994. Neogene gravity tectonics and depositional processes on the deep Niger Delta continental margins. Marine and Petroleum Geology 11, 321–346.

Davies, R.J., Turner, J.D., Underhill, J.R., 2001. Sequential dip-slip fault movement during rifting: a new model of the trilete North Sea rift system. Petroleum Geoscience 7, 371–388.

Demercian, S., Szatmari, P., Cobbold, P.R., 1993. Style and pattern of salt diapirs due to thin-skinned gravitational gliding, Campos and Santos basins, offshore Brazil. Tectonophysics 228, 393–433.

Dutton, D.M., Lister, D., Trudgill, B.D., Pedro, K., 2004. Three-dimensional geometry and displacement configuration of a fault array from a raft system, Lower Congo Basin, offshore Angola: implications for the Neogene turbidite play. In: Davies, R.J., Cartwright, J.A., Stewart, S.A., Lappin, M., Underhill, J.R. (Eds.), 3D Seismic Technology: Application to the Exploration of Sedimentary Basins. The Geological Society of London, Memoir, vol. 29, pp. 133–142.

Duval, B., Cramez, C., Jackson, M.P.A., 1992. Raft tectonics in the Kwanza Basin, Angola. Marine and Petroleum Geology 9, 389–404.

Fletcher, K.J., 2003. The South Brae field, blocks 16/07a, 16/07b, UK North Sea. In: Gluyas, J.G., Hichens, H.M. (Eds.), United Kingdom Oil and Gas Fields, Commemorative Millennium Volume. Geological Society of London, Memoir, vol. 20, pp. 211–221.

Fletcher, K.J., 2003. The central Brae field, blocks 16/07a, 16/07b, UK North Sea. In: Gluyas, J.G., Hichens, H.M. (Eds.), United Kingdom Oil and Gas Fields, Commemorative Millennium Volume. Geological Society of London, Memoir, vol. 20, pp. 183–190.

Fisher, M.J., Mudge, D.C., 1990. Triassic. In: Glennie, K.W. (Ed.), Introduction to the Petroleum Geology of the North Sea. Blackwell, Oxford, pp. 191–218.

Fisher, M.J., Mudge, D.C., 1998. Triassic. In: Glennie, K.W. (Ed.), Petroleum Geology of the North Sea; Basin Concepts and Recent Advances. Blackwell, Oxford, pp. 212–244.

Fraser, S.I., Robinson, A.M., Johnson, H.D., Underhill, J.R., Kadolsky, D.G.A., Connell, R., Johannessen, P., Ravnas, R., 2003. Upper Jurassic. In: Evans, D., Graham, C., Armour, A., Bathurst, P. (Eds.), The Millennium Atlas: Petroleum Geology of the Central and Northern North Sea. The Geological Society of London, pp. 157–189.

Frostick, L.E., Linsey, T.K., Reid, I., 1992. Tectonic and climatic control on Triassic sedimentation in the Beryl Basin, northern North Sea. Journal of the Geological Society of London 149, 13–26.

Gabrielsen, R.H., Færseth, R.B., Steel, R.J., Idil, S., Kløvjan, O.S., 1990. Architectural styles of basin fill in the northern Viking Graben. In: Blundell, D.J., Gibbs, A.D. (Eds.), Tectonic Evolution of the North Sea Rifts. International Lithosphere Programme Publication, vol. 81, pp. 158–179.

Gaullier, V., Brun, J.P., Guérin, G., Lecanu, H., 1993. Raft tectonics: the effects of residual topography below a salt décollement. Tectonophysics 228, 363–381.

Gawthorpe, R.L., Leeder, M.R., 2000. Tectono-sedimentary evolution of active extensional basins. Basin Research 12, 195–218.

Gawthorpe, R.L., Jackson, C.A.-L., Young, M.J., Sharp, I.R., Moustafa, A.R., Leppard, C.W., 2003. Normal fault growth, displacement localisation and the evolution of normal fault populations: the Hammam Faraun fault block, Suez rift, Egypt. Journal of Structural Geology 25, 883–895.

Glennie, K.W., 1984. Early Permian – Rotliegend. In: Glennie, K.W. (Ed.), Introduction to the Petroleum Geology of the North Sea. Blackwell Scientific, London.

Glennie, K.W., 1990. Outline of North Sea history and structural framework. In: Glennie, K.W. (Ed.), Introduction to the Petroleum Geology of the North Sea. Blackwell, Oxford, pp. 34–77.

Gibbs, A.D., 1984. Structural evolution of extensional basin margins. Journal of the Geological Society of London 141, 609–620.

Harris, J.P., Fowler, R.M., 1987. Enhanced prospectivity of the Mid-Late Jurassic sediments of the South Viking Graben, northern North Sea. In: Brooks, J., Glennie, K. (Eds.), Petroleum Geology of Northwest Europe: Proceedings of the Fourth Conference. Graham & Trotman, London, pp. 879–898.

Harvey, M.J., Stewart, S.A., 1998. Influence of salt on the structural evolution of the channel basin. In: Underhill, J.R. (Ed.), The development, evolution and

petroleum geology of the Wessex Basin. Geological Society, London, Special Publications, vol. 133, pp. 241–266.
Hodgson, N.A., Farnsworth, J., Fraser, A.J., 1992. Salt-related tectonics, sedimentation and hydrocarbon plays in the Central Graben, North Sea, UKCS. In: Hardman, R.F.P. (Ed.), Exploration Britain: Insights for the Next Decade. Geological Society, London, Special Publications, vol. 67, pp. 31–63.
Imber, J., Childs, C., Nell, P.A.R., Walsh, J.J., Hodgetts, D., Flint, S.S., 2002. Hangingwall fault kinematics and footwall collapse in listric growth fault systems. Journal of Structural Geology 25, 197–208.
Jackson, C.A.-L., Larsen, E., 2008. Timing basin inversion using 3D seismic and well data: a case study from the South Viking Graben, offshore Norway. Basin Research.
Lundin, E.R., 1992. Thin-skinned extensional tectonics on a salt detachment, northern Kwanza Basin, Angola. Marine and Petroleum Geology 9, 405–411.
McClay, K.R., 1990. Extensional fault systems in sedimentary basins: a review of analogue modelling studies. Marine and Petroleum Geology 7, 206–233.
McLeod, A.E., Dawers, N.H., Underhill, J.R., 2000. The propagation and linkage of normal fault: insights from the Strathspey–Brent–Statfjord fault array, northern North Sea. Basin Research 12, 263–284.
McClure, N.M., Brown, A.A., 1992. A subtle Upper Jurassic submarine fan trap in the South Viking Graben, United Kingdom, North Sea. In: Halbouty, M. (Ed.), Giant Oil and Gas Fields of the Decade (1978–1988). American Association of Petroleum Geologists Memoir, vol. 54, pp. 307–322.
Nilsen, K.T., Vendeville, B.C., Johansen, J.T., 1995. Influence of regional tectonics on halokinesis in the Nordkapp basin, Barents Sea. In: Jackson, M.P.A., Roberts, D.G., Snelson, S. (Eds.), Salt Tectonics: a Global Perspective. American Association of Petroleum Geologists Memoir, vol. 65, pp. 413–436.
Peacock, D.C.P., Sanderson, D.J., 1994. Geometry and development of relay ramps in normal fault zones. Bulletin of the American Association of Petroleum Geologists 81, 82–99.
Penge, J., Taylor, B., Huckerby, J.A., Munns, J.W., 1993. Extension and salt tectonics in the East Central Graben. In: Parker, J.R. (Ed.), Petroleum Geology of Northwest Europe: Proceedings of the Fourth Conference. Geological Society of London, pp. 1197–1210.
Penge, J., Munns, J.W., Taylor, B., Windle, T.M.F., 1999. Rift–raft tectonics: examples of gravitational tectonics from the Zechstein basins of northwest Europe. In: Fleet, A.J., Boldy, S.A.R. (Eds.), Petroleum Geology of Northwest Europe: Proceedings of the Fifth Conference. Geological Society of London, pp. 201–213.
Pegrum, R.M., Ljones, T.E., 1984. 15/9 Gamma gas field offshore Norway, new trap type for North Sea Basin with regional structural implications. American Association of Petroleum Geologists Bulletin 68, 874–902.
Petersen, K., Clausen, O.R., Korstgård, J.A., 1992. Evolution of a salt-related listric growth fault near the D-1 well, block 5605, Danish North Sea, displacement history and salt kinematics. Journal of Structural Geology 14, 565–577.
Prosser, S., 1993. Rift-related depositional systems and their seismic expression. In: Williams, G., Dobbs, A. (Eds.), Tectonics and seismic sequence stratigraphy. Geological Society, London, Special Publications, vol. 71, pp. 35–66.
Roberts, A., Yielding, G., 1994. Continental extensional tectonics. In: Hancock, P.L. (Ed.), Continental Deformation. Pergamon Press, Oxford, pp. 223–250.
Rouby, D., Raillard, S., Guillocheau, F., Bouroullec, R., Nalpas, T., 2002. Kinematics of growth fault/raft systems on the West African margin using 3-D restoration. Journal of Structural Geology 24, 783–796.
Schlische, R.W., Anders, M.H., 1996. Stratigraphic effects and tectonic implications of the growth of normal faults and extensional basins. In: Beratan, K.K. (Ed.), Reconstructing the History of Basin and Range Extension Using Sedimentology and Stratigraphy. Geological Society, America, Special Paper, vol. 33, pp. 183–203.
Sharp, I.R., Gawthorpe, R.L., Armstrong, B., Underhill, J.R., 2000. Propagation history and passive rotation of mesoscale normal faults: implications for synrift stratigraphic development. Basin Research 12, 285–305.
Spathopolous, F., 1996. An insight on salt tectonics in the Angola Basin, South Atlantic. In: Alsop, G.I., Blundell, D.J., Davison, I. (Eds.), Salt Tectonics. Geological Society, London, Special Publications, vol. 100, pp. 153–174.
Stewart, S.A., Coward, M.P., 1995. Synthesis of salt tectonics in the southern North Sea, UK. Marine and Petroleum Geology 5, 457–475.
Stewart, S.A., Fraser, S.I., Cartwright, J.A., Clark, J., Johnson, H.D., 1999. Controls on upper Jurassic sediment distribution in the Durward–Dauntless area, UK Blocks 21/1 l, 21/16. In: Fleet, A.J., Boldy, S.A.R. (Eds.), Petroleum Geology of Northwest Europe: Proceedings of the Fifth Conference. Geological Society of London, pp. 879–896.
Taylor, S.K., Nicol, A., Walsh, J.J., 2008. Displacement loss on growth faults due to sediment compaction. Journal of Structural Geology 30, 394–405.
Thomas, D.W., Coward, M.P., 1996. Mesozoic regional tectonics and South Viking Graben formation: evidence for localized thin-skinned detachments during rift development and inversion. Marine and Petroleum Geology 13, 149–177.
Underhill, J.R., Partington, M.A., 1993. Jurassic thermal doming and deflation in the North Sea: implications of the sequence stratigraphic evidence. In: Parker, J.R. (Ed.), Petroleum Geology of Northwest Europe: Proceedings of the Fourth Conference. Geological Society of London, pp. 337–345.
Underhill, J.R., Partington, M.A., 1994. Use of genetic sequence stratigraphy in determining a regional tectonic control on the "Mid-Cimmerian Unconformity": implications for North Sea basin development. In: Weimer, P., Posamentier, H.W. (Eds.), Siliciclastic Sequence Stratigraphy. American Association of Petroleum Geologists Memoir, vol. 58, pp. 449–484.
Young, M.J., Gawthorpe, R.L., Hardy, S., 2001. Growth and linkage of a segmented normal fault zone; the Late Jurassic Murchison–Statfjord North Fault, northern North Sea. Journal of Structural Geology 23, 1933–1952.
Ziegler, P.A., 1990. Tectonic and palaeogeographic development of the North Sea rift system. In: Blundell, D.J., Gibbs, A.D. (Eds.), Tectonic Evolution of the North Sea Rifts. International Lithosphere Programme Publication, vol. 81, pp. 1–36.